



Analyzing the effect of anisotropic spatial correlations of earthquake intensity measures on the result of seismic risk and resilience assessment of the portfolio of buildings and infrastructure systems

Morteza Abbasnejadfar¹ · Morteza Bastami¹  · Afshin Fallah² · Alireza Garakaninezhad³

Received: 19 June 2021 / Accepted: 7 August 2021 / Published online: 17 August 2021
© The Author(s), under exclusive licence to Springer Nature B.V. 2021

Abstract

The seismic risk assessment of spatially distributed assets requires a seismic hazard that considers the spatial correlations of earthquake intensity measures (IMs). Several spatial correlation models have been developed to address this concern, but the majority of existing models are based on the hypothesis of isotropy. Recent investigations revealed that the assumption of isotropy is not generally valid, and the anisotropy condition should be taken into account when considering the spatial correlations of earthquake IMs. On the other hand, it is necessary to investigate the significance of the inclusion of anisotropy in seismic risk and resiliency assessment. The main objective of the current study is to address this issue using three different spatial correlation models. Two of them are based on the linear model of coregionalization method, which describes the spatial correlation of earthquake IMs from the isotropy point of view. The third model is based on the latent dimensions method, which can take the anisotropy into account. The results of the current study reveal that the ignorance of anisotropy of spatial correlations of earthquake IMs causes unrealistic loss estimation and leads to inaccurate resilience assessment of spatially distributed assets and systems. It is demonstrated specifically that the isotropic models generally overestimate the infrequent loss values which is on the safe side, but underestimate the frequent loss values that is non-conservative.

Keywords Spatial correlation · Anisotropy · Seismic hazard · Risk assessment · Resilience

✉ Morteza Bastami
m.bastami@iiees.ac.ir

¹ International Institute of Earthquake Engineering and Seismology (IIEES), Tehran, Iran

² Department of Statistics, Imam Khomeini International University (IKIU), Qazvin, Iran

³ Department of Civil Engineering, Faculty of Engineering, University of Jiroft, Jiroft, Kerman, Iran

1 Introduction

Urban areas, as the most significant habitat of human communities, are composed of different spatially distributed assets. The urban assets include both the infrastructure systems as life-lines of communities and assemblies of small properties such as residential buildings with considerable aggregated value. Both of these assets are concerned with spatial distribution, a central concept in risk assessment and urban planning. These assets are generally impacted by a variety of destructive events; the most severe of those would be earthquakes, which can cause significant losses. As a result, different stockholders at the city and country levels, insurance companies, and international organizations are interested in assessing the seismic risk and resilience of spatially distributed assets.

The seismic risk assessment framework is composed of three modules of 1-seismic hazard, 2- exposure level, and 3- earthquake vulnerability. The seismic hazard module has a significant effect on the estimated loss values. Previous researches have shown that the spatial correlations should be considered in estimating earthquake intensity measures (IMs), and failure to incorporate the spatial correlation of earthquake IMs would result in erroneous loss estimations (Bastami 2007; Lee and Kiremidjian 2007; Park et al. 2007; Goda and Hong 2008b; Weatherill et al. 2015). In this regard, different spatial correlation models have been proposed by different research works. A comprehensive review of the models published until 2019 can be found in Schiappapietra and Douglas (2020) and Abbasnejadfar et al. (2020). The main objective of these models is to determine a correlation range for earthquake IMs, which is defined as a distance beyond which the values of IMs' random field could be considered uncorrelated. Most of the existing spatial correlation models are based on the hypothesis of isotropy, which implies that the spatial correlation range is the same in all directions.

Garakaninezhad and Bastami (2017) demonstrated that the isotropy of spatial correlations of earthquake IMs is not generally a valid hypothesis. Taking this finding into consideration, Abbasnejadfar et al. (2020) proposed a new spatial correlation model of multiple earthquake IMs based on the latent dimensions method. With several isotropic and anisotropic spatial correlation models in hand, the question is how important anisotropy considerations are in the spatial correlation of earthquake IMs. The main objective of the current research work is to address this question through the employment of various spatial correlation models and different scenarios of exposure models of portfolio of buildings and transportation network.

2 Spatial correlation models of earthquake intensity measure

Ground motion models (GMM) are statistical tools that are employed to estimate earthquake IMs. The general form of GMMs are as:

$$\ln(Y_{ij}) = \ln(\overline{Y_{ij}}) + \delta_{ij}, \quad (1)$$

where Y_{ij} is the amount of estimated IM at point i given earthquake event j , $\overline{Y_{ij}}$ is the median value of IM that is determined by ground motion prediction equation (GMPE) and δ_{ij} is the residual term of the model that represents the stochastic variability of IM. As demonstrated in equation (2), the residual term of equation (1) is comprised of the inter-event (η_j) and intra-event (ε_{ij}) residual terms.

$$\delta_{ij} = \eta_j + \varepsilon_{ij}. \quad (2)$$

The inter-event residual term represents event-to-event stochastic variability of IM that can be considered a normal random variable with zero mean and standard deviation of τ . On the other hand, the intra-event residual term represents the point-to-point stochastic variability of IM. According to Jayaram and Baker (2008) a vector of intra-event residuals at n spatially distributed location in the earthquake event j ($\mathbf{e}_j = (\epsilon_{1j}, \epsilon_{2j}, \dots, \epsilon_{nj})$) follows a multivariate normal distribution and the \mathbf{e}_j can be considered as a realization of a Gaussian random field with a mean of zero and a standard deviation of σ .

Different methods can be addressed in order to estimate the values of a random field at spatially distributed locations (Cressie 1993); among them, the Cholesky decomposition method is one of the most used approaches in seismology and earthquake engineering (Jayaram 2010; Weatherill et al. 2015). By using this method, the vector of random field values ($\mathbf{Z}_{n \times 1}$) at n spatially distributed locations can be modeled as:

$$\mathbf{Z} = \boldsymbol{\mu} + \mathbf{L}\boldsymbol{\xi}, \tag{3}$$

where $\boldsymbol{\mu} = \{\mu(\mathbf{s}_1), \dots, \mu(\mathbf{s}_n)\}'$ is the vector of mean values of the random field at spatially distributed locations $\mathbf{s}_1, \dots, \mathbf{s}_n$; $\boldsymbol{\xi} = \{\xi(\mathbf{s}_1), \dots, \xi(\mathbf{s}_n)\}'$ is an n -dimensional vector of uncorrelated random numbers with standard normal distribution, and \mathbf{L} is an $n \times n$ lower triangular matrix that is obtained from Cholesky decomposition of covariance matrix $\boldsymbol{\Sigma}$ of the interested random field as presented in equation (4).

$$\boldsymbol{\Sigma} = \mathbf{L}\mathbf{L}^T. \tag{4}$$

In order to be used in the context of the Cholesky decomposition method, the covariance matrix $\boldsymbol{\Sigma}$ must be non-negative definite. The requirement for a non-negative definite covariance matrix also arises from the fact that the correlation coefficient values between different random variables at different locations must always be non-negative, which can only be achieved by a positive-semidefinite covariance matrix.

The earliest studies on the spatial correlations of intra-event residuals of earthquake IMs were based on the variability of correlation coefficient of intra-event residuals as a function of separation distances; hence various models have been proposed addressing this subject (Boore et al. 2003; Wang and Takada 2005; Goda and Hong 2008a; Goda and Atkinson 2009). The principles and methods of spatial statistics, such as variogram, covariogram, and correlogram concepts (see Cressie (1993) for more information), have been employed in the subsequent studies (e.g., Jayaram and Baker (2009); Esposito and Iervolino (2011, 2012); Du and Wang (2013), etc.) to achieve a reliable and valid covariance matrix of intra-event residuals.

Before the study of Garakaninezhad and Bastami (2017), the random field of intra-event residuals is assumed to be second-ordered-stationary (Wang and Takada 2005) and isotropic (Jayaram and Baker 2009). Under the assumption of stationarity, 1- the mentioned random field is supposed to have an equal mean value regardless of location; 2- the covariance of random field values at two different locations (\mathbf{s}_1 and \mathbf{s}_2) depends only on the distance of interested locations (\mathbf{s}_1 - \mathbf{s}_2). On the other hand, under the assumption of isotropy, the range of spatial correlations is expected to be equal in all directions. Garakaninezhad and Bastami (2017), by using the peak ground acceleration (PGA) and spectral accelerations (SA) of record stations of several earthquake events and by employing a non-parametric statistical test, demonstrated that the hypothesis of isotropy is not generally valid.

Multiple IMs of a particular earthquake scenario may be required when assessing the seismic risk of spatially distributed assets. For instance, a portfolio of buildings generally consists of various typologies and heights; therefore, the seismic risk assessment needs

SAs of different periods if the utilized fragility or vulnerability curves are based on SAs. In such cases, the spatial cross-correlations of IMs should also be considered, in addition to their marginal spatial correlations.

Jayaram and Baker (2008) demonstrated that the set of spatially distributed residuals of SAs at multiple periods could be represented by a multivariate Gaussian distribution. According to Cressie (1993), the cross-covariance function for the second-ordered stationary multivariate (k -variate) random field of

$$\left\{ \mathbf{e}'(\mathbf{s}) = [\varepsilon'_1(\mathbf{s}), \dots, \varepsilon'_k(\mathbf{s})]' : \mathbf{s} \in \mathbb{R}^2 \right\}, \tag{5}$$

can be defined as:

$$\begin{aligned} C_{\alpha\beta}(\mathbf{h}) &= \text{Cov}(\varepsilon'_\alpha(\mathbf{s}), \varepsilon'_\beta(\mathbf{s} + \mathbf{h})) \\ &= \text{E} \left[(\varepsilon'_\alpha(\mathbf{s}) - \text{E}[\varepsilon'_\alpha]) (\varepsilon'_\beta(\mathbf{s} + \mathbf{h}) - \text{E}[\varepsilon'_\beta]) \right], \alpha, \beta = 1, \dots, k, \end{aligned} \tag{6}$$

where $\text{Cov}[\cdot]$ and $\text{E}[\cdot]$ represent covariance and expectation functions, respectively; \mathbf{s} represents the location, and \mathbf{h} is the lag vector. By utilizing equation (6), the cross-correlation function could be obtained as presented in equation (7).

$$\rho_{\alpha\beta}(\mathbf{h}) = \frac{C_{\alpha\beta}(\mathbf{h})}{\{C_{\alpha\alpha}(\mathbf{0}) \times C_{\beta\beta}(\mathbf{0})\}^{1/2}}. \tag{7}$$

The covariance $\mathbf{C}(\mathbf{h})$ and correlation $\mathbf{R}(\mathbf{h})$ matrices are $k \times k$ matrices (for a k -variate random field) that are composed of the $C_{\alpha\beta}(\mathbf{h})$ and $\rho_{\alpha\beta}(\mathbf{h})$ for different pairs of components α and β . The diagonal elements of these matrixes represent the marginal covariance and correlation functions, and off-diagonal elements represent cross-covariance and cross-correlation functions for different pairs of components.

The covariance matrix of an event e for n spatially distributed sites (Σ_e) can then be generated using the $\mathbf{C}(\mathbf{h})$ matrix considering different \mathbf{h} values obtained from different pairs of locations, as shown in equation (8).

$$\Sigma_e = \begin{bmatrix} \mathbf{C}(\mathbf{h}_{s_1, s_1}) & \dots & \mathbf{C}(\mathbf{h}_{s_1, s_n}) \\ \vdots & \ddots & \vdots \\ \mathbf{C}(\mathbf{h}_{s_n, s_1}) & \dots & \mathbf{C}(\mathbf{h}_{s_n, s_n}) \end{bmatrix}_{nk \times nk} \tag{8}$$

The correlated vector of the k -variate random variable at n spatially distributed sites ($\mathbf{E}' = \{\mathbf{e}'(s_1)^T, \dots, \mathbf{e}'(s_n)^T\}^T$, $\mathbf{e}' = \{\varepsilon'_1, \dots, \varepsilon'_k\}^T$) can be simulated by knowing the covariance matrix Σ_e and utilizing equations (3) and (4).

As mentioned in the previous paragraphs, the covariance matrix Σ_e must be non-negative definite. Generally, generating a non-negative definite covariance matrix Σ_e for a multivariate random field is a challenging problem in spatial statistics and its applications. Several researchers have proposed different cross-correlation models in order to generate a valid non-negative definite covariance matrix of multiple intra-event residuals of earthquake events. One of the common approaches in this respect is the linear model of coregionalization (LMC) method (Loth and Baker 2013; Wang and Du 2013; Garakaninezhad and Bastami 2019). This method employs a linear combination of r univariate random fields to define a multivariate random field as presented in equation (9).

$$\Phi(h) = \sum_{l=1}^r \mathbf{B}^l \phi_l(h) \tag{9}$$

In equation (9), $\Phi(h)$ could be semivariogram, covariance or correlation matrix of the multivariate random field, $\phi_l(h)$ is the l th univariate semivariogram, covariance or correlation function, accordingly, and \mathbf{B}^l is the coregionalization matrix related to l th model.

Loth and Baker (2013) utilized the LMC method to define a predictive model for covariance matrix function of different SAs from 0.01 to 1.0 s. In the mentioned study, the proposed covariance matrix function is in the form of:

$$\mathbf{C}(h) = \mathbf{B}^1 \exp\left(\frac{-3h}{20}\right) + \mathbf{B}^2 \exp\left(\frac{-3h}{70}\right) + \mathbf{B}^3 K_{h=0} \tag{10}$$

where $K_{h=0}$ is the indicator function that equals to 1 at $h = 0$ and equals to 0 at $h \neq 0$. Also, coregionalization matrices \mathbf{B}^1 , \mathbf{B}^2 , and \mathbf{B}^3 are obtained based on the average values of fitted coregionalization matrices of eight earthquake events. As can be seen in equation (10), the covariance matrix function of the multivariate random field proposed by Loth and Baker (2013) is mainly composed of two univariate covariance functions with correlation ranges of 20 and 70 km. Moreover, the term $\mathbf{B}^3 K_{h=0}$ is employed to take account of the nugget effect.

The spatial cross-correlation of intra-event residuals of earthquake IMs is also investigated by Wang and Du (2013). Two sets of IMs are considered in the mentioned study. The first set is composed of PGA, PGV and I_A , and the second set consists of SAs at six periods ranging from 0.01 to 5 s. Wang and Du (2013) utilized the LMC method, and the correlation matrix function is proposed as:

$$\mathbf{R}(h) = \mathbf{P}^1 \exp\left(\frac{-3h}{10}\right) + \mathbf{P}^2 \exp\left(\frac{-3h}{70}\right). \tag{11}$$

The models of Wang and Du (2013) and Loth and Baker (2013) are different in several aspects. 1-The correlation range of the short-range basic function of the LMC method is considered 10 km in the model of Wang and Du (2013), which is less than the 20 km considered in Loth and Baker (2013). 2- Wang and Du (2013) concluded that the nugget effect is not significant in the correlation function of the intra-event residuals of earthquake IMs, and consequently, the nugget effect is not included in the proposed model, but the model of Loth and Baker (2013) consists of the nugget effect term. 3- The main difference between the mentioned models is that the model of Wang and Du (2013) considers the effects of regional site conditions when defining the coregionalization matrices. As a result, the coregionalization matrices \mathbf{P}^1 and \mathbf{P}^2 are defined as functions of correlation range of V_{S30} ($R_{V_{S30}}$). This is in contrast to the model of Loth and Baker (2013), which ignores local soil type conditions and suggests the same covariance function matrices for different sites with different correlation ranges.

The previously mentioned multivariate covariance (correlation) models are generated based on the isotropy assumption of spatial correlations of earthquake IMs. Abbasnejad-fard et al. (2020) proposed a predictive model based on the latent dimensions (LD) method for defining the covariance matrix of the multivariate random field of intra-event residuals of multiple earthquake IMs accounting for spatial anisotropy.

The study of Abbasnejad-fard et al. (2020) focused on two sets of earthquake IMs: the first set includes PGA, PGV, and PGD, and the second set comprises SAs at multiple

periods. Using the LD method, the multivariate random field, which is originally defined in a 2-dimensional space, is considered as a univariate random field with an added latent dimension (3-dimensional space). In this regard, the cross-covariance function of two components of multivariate random field α and β ($C_{\alpha\beta}(\mathbf{s}_1, \mathbf{s}_2) : \mathbf{s}_1, \mathbf{s}_2 \in \mathbb{R}^2$) is considered as $C((\mathbf{s}_1, \xi_\alpha), (\mathbf{s}_2, \xi_\beta))$, which is the covariance function of a univariate random field that is defined in \mathbb{R}^{2+1} space. Using this conversion, the existing valid covariance functions that are defined for anisotropic univariate random fields could be implemented to generate a non-negative definite covariance matrix Σ_e . More details about the LD method can be found in Apanasovich and Genton (2010). Abbasnejadfar et al. (2020) utilized the covariance function of equation (12) introduced by Apanasovich and Genton (2010), which is capable of incorporating the anisotropy.

$$C_{\alpha\beta}(\mathbf{h}) = C(\mathbf{h}, v_{\alpha\beta} - \gamma \boldsymbol{\omega}^T \mathbf{h}) = \frac{\sigma_{\alpha\beta}}{|v_{\alpha\beta} - \gamma \boldsymbol{\omega}^T \mathbf{h}| + 1} \exp \left\{ - \frac{a \|\mathbf{h}\|}{\left(|v_{\alpha\beta} - \gamma \boldsymbol{\omega}^T \mathbf{h}| + 1 \right)^{1/2}} \right\} \tag{12}$$

In equation (12), α and β represent the intra-event residuals of different earthquake IMs, $\mathbf{h} = \mathbf{s}_i - \mathbf{s}_j$ is the distance vector of points i and j , $\boldsymbol{\omega}^T = \{\omega_1, \omega_2\}^T$ is the anisotropy direction vector, $\sigma_{\alpha\beta}$ is the variance parameter, $\gamma \geq 0$ is the anisotropy ratio parameter, and a is the parameter of anisotropy range. The anisotropy range represents the maximum correlation range of an anisotropic model in different directions, while the anisotropy ratio represents the ratio of the highest to lowest correlation range in different directions. Instead of latent dimensions (ξ_α, ξ_β) , the latent distance parameter $v_{\alpha\beta} = \xi_\alpha - \xi_\beta$ is used in the equation (12); therefore, the shorter latent distance parameter $v_{\alpha\beta}$ represents greater cross-correlation between components α and β , and vice versa. By replacing β with α , the auto-covariance function can be developed as per equation (13), considering that the latent distance of each variable with itself equals to zero.

$$C_{\alpha\alpha}(\mathbf{h}) = \frac{\sigma_{\alpha\alpha}}{|\gamma \boldsymbol{\omega}^T \mathbf{h}| + 1} \exp \left\{ - \frac{a \|\mathbf{h}\|}{\left(|\gamma \boldsymbol{\omega}^T \mathbf{h}| + 1 \right)^{1/2}} \right\} \tag{13}$$

According to Abbasnejadfar et al. (2020), the anisotropy properties of the LD model presented in equation (12) mainly is a function of anisotropy properties of the local soil condition of the investigated site. In this regard, it is demonstrated that the anisotropy direction of GMF of earthquake IMs has a strong agreement with the anisotropy direction of local soil condition and the anisotropy ratio and anisotropy range of the earthquake IMs are defined as a function of those parameters of the local soil condition.

However, as noted in Abbasnejadfar et al. (2020), the anisotropy properties of earthquake IMs' GMF may be influenced by some other parameters, including the physical parameters of the earthquake source or propagation path. For instance, Garakaninezhad and Bastami (2017), by using the directional semivariogram, demonstrated that in some cases of recorded earthquake IMs, the physical parameters of earthquake source like strike direction have good agreement with the anisotropy direction of the univariate GMF earthquake IMs. As another instance, Schiappapietra and Smerzini (2021), by using "a set of broadband physics-based ground motion simulations", demonstrated that the slip direction and geometry of causative fault affect the anisotropy of spatial correlations of earthquake IMs.

Despite the mentioned evidence, the effect of source and path on anisotropy properties of GMF of IMs are not extensively included in the existing predictive models of intra-event residuals and the few studies and models that have addressed this subject are considered the univariate random field of IMs. According to Abbasnejadfar et al. (2020), introducing any new parameter in spatial correlation models necessitates statistical inference; therefore, adequate data should be supplied. This is despite the fact that there is now insufficient real-world data from earthquake events to include the effects of source and path. For this reason, using the earthquake events simulation method can be considered as a reliable treatment of this issue. In this regard, existing models (particularly multivariate models) are expected to be upgraded to include the source and path effects on anisotropic properties of earthquake IMs, or new models to be developed to consider the effects of source, path, and site simultaneously. According to the discussion mentioned above, a general framework is presented in Fig. 1 on how an anisotropic model could be implemented in a Monte Carlo based probabilistic seismic risk assessment process considering the physical characteristics of regional site condition and multiple source and path scenarios.

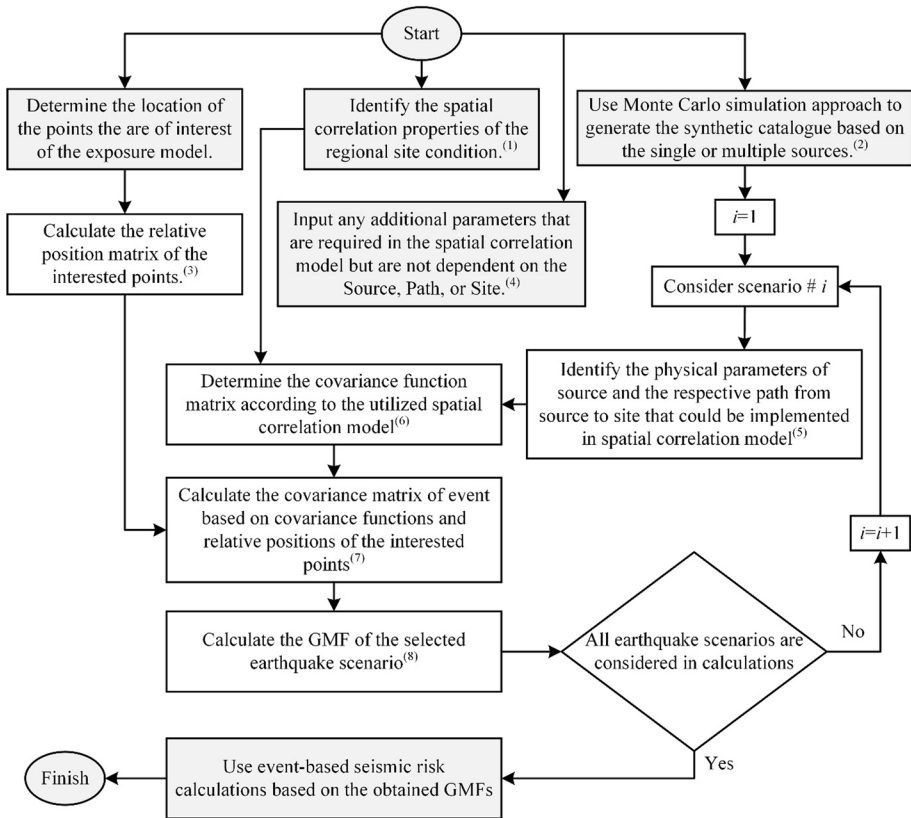
3 A general perspective of the investigation method

As mentioned previously, the main objective of the current study is to investigate how taking into account anisotropy in spatial correlations of earthquake IMs affects the outcomes of seismic risk and resilience assessment of spatially distributed assets. To achieve this objective, the spatial correlation model proposed by Abbasnejadfar et al. (2020), which is based on the latent dimensions (LD) method, are utilized besides the models proposed by Loth and Baker (2013) and Wang and Du (2013), that are based on the linear model of coregionalization (LMC) method.

The current study takes into account two types of spatially distributed assets. The first consists of various scenarios of a portfolio of buildings distributed across an urban area, and the second type of considered assets is a highway-bridge transportation network. The main objective of considering the mentioned inventory types is to study the effect of various spatial correlation models of earthquake IMs on the outcome of seismic risk assessment. Furthermore, alternative building distribution scenarios in terms of building characteristics are studied in order to investigate the effect of the presence of a trend in the spatial distribution of building typologies on the results of seismic risk assessment. The second type of asset is used as a representative example of spatially distributed infrastructure systems that, besides having a spatial distribution feature, forms a linked network of components that requires a connectivity analysis. More details about the specifications of the mentioned assets are discussed in the following sections.

3.1 Description of the study area and earthquake source

Figure 2 provides a schematic view of the Study Area, City Area, and the seismic source. The City Area borders represent the spatial bounds of the assumed distribution of residential buildings in the first case study. The wider border, dubbed the Study Area encompasses a geographic limit where the assumed transportation network is located.



⁽¹⁾ Mainly the anisotropy properties of the spatial correlations of regional site condition in terms of V_{S30} (e.g. anisotropy direction, anisotropy ratio, anisotropy range) are of interest. As an example of how these parameters might be used, see Abbasnejadfar et al. (2020). This step can be skipped if the regional site condition is not included in the model.

⁽²⁾ In this step several stochastic are generated based on the seismicity and physical characteristics of the sources. The generated catalogue consists of different variables of an earthquake event, some of which may be incorporated in the utilized spatial correlation model and may have considerable effects on the anisotropy of spatial correlations of IMs. See Crowley and Bommer (2006) for more descriptions about Monte Carlo simulation.

⁽³⁾ Given n spatially distributed locations determined in the preceding step, the relative distance matrix (H) will have $n \times n$ dimensions, with each of its components being a vector connecting two locations determined in the exposure model.

⁽⁴⁾ e.g. the latent distance parameters proposed by Abbasnejadfar et al. (2020).

⁽⁵⁾ See Schiappapietra and Smerzini (2021) to see how the physical parameters of source can affect the anisotropy properties of spatial correlations of IMs. The application of the physical parameters of source in the spatial correlation models can be found in Garakaninezhad and Bastami (2017). This step can be skipped if the physical parameters of source or path are not included in the model.

⁽⁶⁾ More information can be found in the discussions that follow equation 7.

⁽⁷⁾ See equation 8 for more information.

⁽⁸⁾ For the objective of this step, equation (1) can be used. See section 2 for more information.

Fig. 1 A general framework for an event-based seismic risk assessment considering the physical characteristics of source, path and site and taking into account the anisotropy of spatial correlations of earthquake IMs

Fig. 2 Schematic view of the relative location of the seismic source, Study Area, and City Area

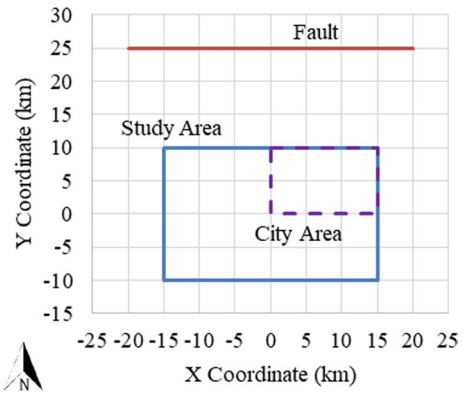


Table 1 Geometric parameters of the assumed seismic source

Parameter name	Parameter value	Unite
Strike Azimuth	90	Degree
Dip Angle	60	Degree
Length	40	km
Width	10	km
Shallowest Depth	(X,Y,Z)=(- 5,3,3)	km

The seismic source in the current investigation is a rupture surface with the geometric parameters shown in Table 1. Figure 2 depicts the fault line as the projection of the shallowest part of the seismic source on the ground surface.

The activity of the seismic source is characterized using the bounded Gutenberg–Richter recurrence law with $m_{\min}=5.5$, $m_{\max}=8$, $\lambda_{m-\min}=0.1$, $b=0.52$. These parameters are delineated from the seismicity of Tehran region as one of the earthquake prone areas around the globe (Tavakoli and Ghafory-Ashtiany 1999; Bastami and Kowsari 2014). The event-based stochastic seismic hazard simulation method based on the Monte-Carlo simulation proposed by Crowley and Bommer (2006) is employed to generate the synthetic catalog of the assumed seismic source. More than 10^6 earthquake events have been simulated, and their consequent ground motion field (GMF) of SAs at three different periods of 0.5 s, 1.0 s, and 2.0 s are obtained using Campbell and Bozorgnia (2014) GMPE. The current study employs four different spatial correlation and cross-correlations models of earthquake IMs as:

1. Uncorrelated model
2. The spatial correlation model proposed by Abbasnejadfar et al. (2020) based on the latent dimensions method (LD)
3. The spatial correlation model proposed by Loth and Baker (2013) based on the linear model of coregionalization method (LMC-LB)
4. The spatial correlation model proposed by Wang and Du (2013) based on the linear model of coregionalization method (LMC-WD)

All of the correlation models (items no. 2–4) can consider the cross-correlations of multiple SAs for different periods. Moreover, the models of Abbasnejadfar et al. (2020) and Wang and Du (2013) are capable of considering the regional site conditions in terms of spatial correlations of V_{s30} values. Also, among the utilized spatial correlation methods, only the LD method can include the anisotropy of spatial correlations in its estimations of GMF.

3.2 Regional site condition scenarios and approaches for implementation of different spatial correlation models

Some of the previous studies demonstrated the significance of regional site conditions on the spatial correlations of earthquake IMs (see Wang and Du (2013); Abbasnejadfar et al. (2020) for more detail). In this regard, three different random fields of soil type (S0, S1, and S2) are generated to take into account the effects of regional site conditions. The simulation of soil type random fields is based on estimating the average shear wave velocity of the 30-m depth portfolio of soil (V_{s30}) in spatially distributed locations.

The random field of V_{s30} value for all simulated scenarios of soil types has an average value of 500 m/s and a standard deviation of 120 m/s. The main difference between the soil type scenarios is their spatial correlation ranges, so that scenario S1 has the widest spatial correlation range among other scenarios, S2 has the smallest range than the other scenarios, and the correlation range of scenario S0 is between the correlation range of scenarios S1 and S2. According to Abbasnejadfar et al. (2020), equation (13) is utilized to generate the covariance matrix of random fields of soil type scenarios considering anisotropy. Table 2 presents the anisotropy parameters of different soil type scenarios, and the variance parameter set to unity. The 2D visualization of the different soil type scenarios is present in Fig. 3. The random field of the uncorrelated soil type is also demonstrated in Fig. 3 to be compared with other scenarios. It should be clarified that the uncorrelated soil type is not used in the current study. By knowing the spatial distribution, the correlation range of V_{s30} value for all scenarios is also calculated without considering the anisotropy. This value is utilized in the model of LMC-WD.

Each of the spatial correlation models described in the previous section is combined with three introduced soil type scenarios to generate 12 scenarios of GMFs, as presented in Table 3. These GMF scenarios are used in seismic risk assessment of the case studies of the spatially distributed buildings and assumed transportation network. A description of correlation models utilized in the current research work has been provided in Sect. 2. As discussed in Sect. 2, the elements of coregionalization matrices of the LMC-LB model are independent of any other parameters, while the coregionalization matrices of the LMC-WD model are functions of correlation range of V_{s30} values ($R_{V_{s30}}$). For this reason, the spatial correlation range of different soil type scenarios are utilized in the GMF calculations based

Table 2 Anisotropy parameters of different soil type scenarios

No	Scenario ID	γ	a (km ⁻¹)	Ani-sotropy direction
1	S0	0.2	0.075	N-S
2	S1	0.2	0.05	N-S
3	S2	0.2	0.1	N-S

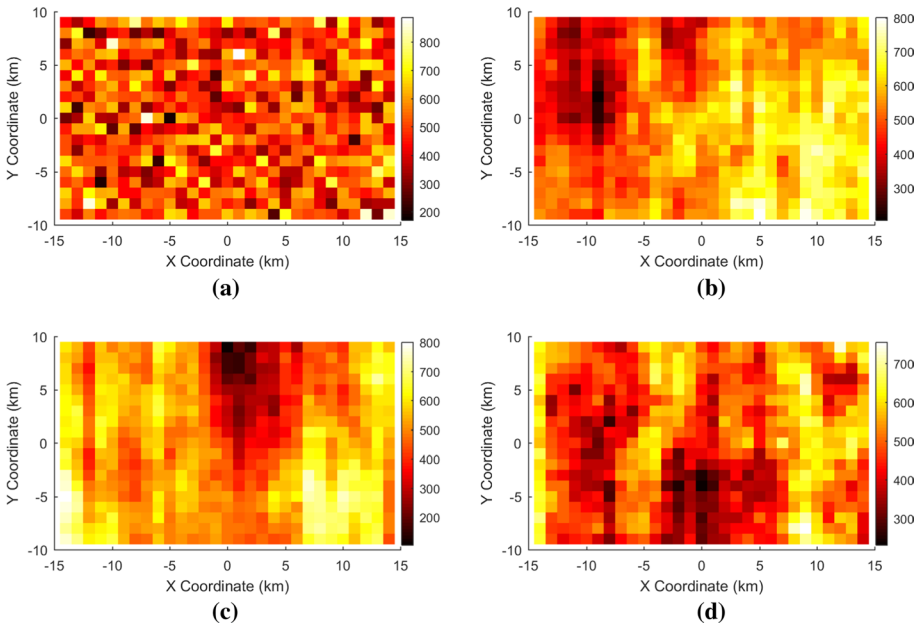


Fig. 3 2D visualization of different soil type scenarios in the study area with different correlation ranges: **a** uncorrelated, **b** scenario S0, **c** scenario S1, **d** scenario S2

Table 3 Designating various hazard analysis scenarios based on soil type scenarios and spatial correlation model

Correlation model	Soil type scenario		
	S1	S0	S2
Uncorrelated	S1H0	S0H0	S2H0
LD	S1H1	S0H1	S2H1
LMC-LB	S1H2	S0H2	S2H2
LMC-WD	S1H3	S0H3	S2H3

on the LMC-WD models. The regional site condition is also a significant factor in the LD model’s GMF estimates. According to the equation (12) different parameters including anisotropy direction ($\omega^T = \{\omega_1, \omega_2\}^T$), anisotropy ratio (γ), anisotropy range (a), and latent distance parameter ($v_{\alpha\beta}$) must be identified to use the LD model in developing covariance functions and calculating multivariate GMF values in spatially distributed locations. Based on the procedure introduced by Abbasnejadfar et al. (2020), the anisotropy direction of the earthquake IMs’ GMF is aligned with the anisotropy direction of regional soil condition. In the current study the anisotropy direction of all soil type scenarios is considered in N-S direction. Moreover, according to Abbasnejadfar et al. (2020), the anisotropy ratio and anisotropy range of earthquake IMs can be obtained using:

$$\gamma = C_\gamma \gamma_{v_{s30}} \tag{14}$$

and

Table 4 Description of exposure model scenarios

Scenario ID	Description
E3	In this scenario, the construction area of each grid is a random variable with mean and standard deviation values of 30,000 and 3000 m ² /4 ha, respectively. Both of the building typologies (STL01 and CON01) are used. STL01 to CON01 built-up area ratio ($BAR_{S/C}$) in each grid has a trend in North–South running direction such that the $BAR_{S/C}$ equals 0.2 in the South and equals 0.8 in the North. The schematic visualization of the built-up area of STL01 building typology per grid is presented in Fig. 4a. The built-up area of CON01 building typology in each grid equals $(1 - BAR_{S/C}) \times$ (built-up area of the grid)
E4	This scenario is similar to E3, except that the $BAR_{S/C}$ trend is in the East–West direction, such that the $BAR_{S/C}$ equals 0.2 in the East and equals 0.8 in the West part of the City Area. (Fig. 4b)
E7	Each grid in Scenario E7 has a built-up area of 30,000 m ² /4 ha. Only STL01 building typology is used in this scenario (uniform built up area using STL01 typology)

$$a = C_a^{-1} a_{V_{s30}}^2 \tag{15}$$

respectively, where $\gamma_{V_{s30}}$ and $a_{V_{s30}}$ are the anisotropy ratio and anisotropy range of local soil conditions (that can be obtained from Table 2) and coefficients C_γ and C_a are defined by Abbasnejadfar et al. (2020) for different pairs of IMs. Also, the latent distance parameters defined by Abbasnejadfar et al. (2020) are utilized in the current study for different pairs of IMs. In this regard, the $v_{\alpha\beta}$ is considered as zero for marginal-covariance models and the values proposed by Abbasnejadfar et al. (2020) are used for cross-covariance models.

The marginal-covariance and cross-covariance functions for different IMs are obtained using the mentioned parameters and equation (12). Then, the event covariance function (Σ_e) is calculated using equation (8). Further steps in calculating GMF values are described in Sect. 2.

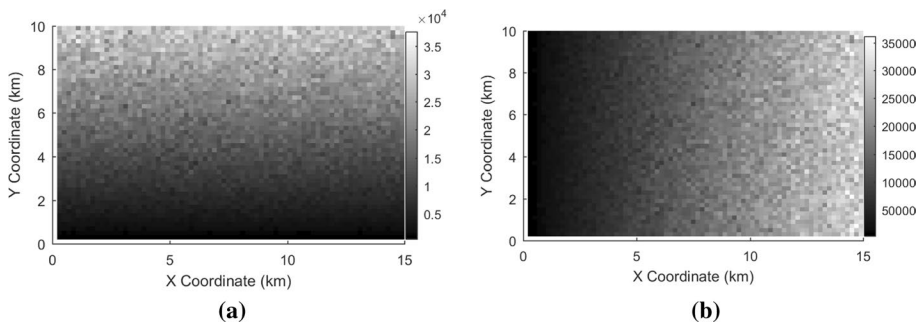


Fig. 4 2D visualization of the defined exposure models, the built-up area of STL01 building per grid are demonstrated as m²/4 ha, **a** scenario E3, **b** scenario E4

4 Seismic risk assessment of the portfolio of buildings

4.1 Description of exposure and vulnerability models

In addition to the hazard module, the introduction of exposure and vulnerability modules is also required to be used in the seismic risk assessment process. In order to achieve the goals outlined in Sect. 3, different scenarios of the building exposure models are defined in the current section. These scenarios are the portfolio of residential buildings that are distributed across a synthetic geographic area known as the City Area (see Figure 1). The exposure scenarios are generated by using two different building typologies (STL01 and CON01). In order to define exposure models, the City Area, which is a 15 km×10 km region, is divided into 200 m×200 m grids (4 ha subdivisions). The exposure models are then created by changing the built-up area of various building typologies in each grid. More information on the various exposure models is provided in Table 4 .

The physical characteristics of the utilized building typologies are described in Table 5. Moreover, the vulnerability curves and characteristics of vulnerability models of specified building typologies are presented in Fig. 5 and Table 6. The defined building typologies and their respective characteristics are selected from the study of Sadeghi et al. (2015), which established the seismic vulnerability curves of typical Iranian building typologies. The two specified building typologies are selected as examples of the common building typologies in an urban area, but it should be noted that the general findings of the current

Table 5 General characteristics of the utilized building typologies (Sadeghi et al. 2015)

Building typology ID	Material type	Lateral load resisting system	Story range	Fundamental natural period	Construction quality [†]
STL01	Steel	Steel bracing	4–7	0.5 s	Low code
CON01	Concrete	Concrete shear wall	≥ 8	1.0 s	High Code

[†] More information on construction quality is available in (Sadeghi et al. 2015)

Fig. 5 Vulnerability curves of utilized building typologies

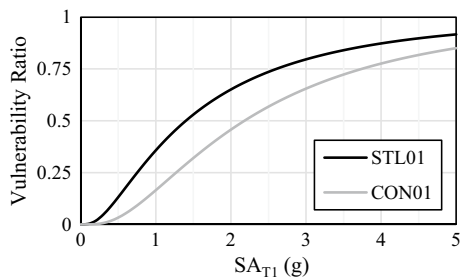


Table 6 Vulnerability model parameters of the utilized building typologies (Sadeghi et al. 2015)

Building typology ID	Earthquake IM	Median SA (g)	Log-standard deviation (β)
STL01	SA(T=0.5 s)	1.40	0.92
CON01	SA(T=1.0 s)	2.18	0.80

study do not depend on the specifications of the selected typologies, and the same results could be achieved by altering the typologies.

4.2 Investigating the effect of considering different spatial correlation models of earthquake IMs on the results of seismic risk assessment of the portfolio of buildings

To investigate the effects of different spatial correlation models of earthquake IMs on seismic risk assessment of spatially distributed buildings, the exposure scenario E7 is used in conjunction with the GMFs generated based on the seismic hazard models of Table 3. For this reason, the Stochastic Event-Based Seismic Risk Calculator of OpenQuake software (Silva et al. 2014) is employed.

The aggregated loss curves of exposure model E7 under the assumptions of soil type scenario S0 are obtained as demonstrated in Fig. 6. In this figure, H0 represents the spatially uncorrelated hazard model, while H1, H2, and H3 stand for the GMFs derived from the LD, LMC-LB and LMC-WD spatial correlation models, respectively. The loss curves are normalized to the total asset value. Moreover, Fig. 6 depicts the ratio of loss values obtained from various hazard models to the loss values of the LD method for different levels of the annual rate of exceedance (ARoE) to provide a better comparative tool.

Although Fig. 6 shows differences in the loss values calculated by different spatial correlation models, the question is whether the loss ratio of different approaches is always equal to what is shown in Fig. 6b and if not then, what factors are primarily responsible for the difference.

To address this question, the soil type scenario is changed, and the exposure scenario E7 is presumed to be located in the soil type environments S1 and S2. As shown in Tables (1, 2) and discussed in Sect.3.2, the difference between three regional site condition scenarios S0, S1, and S2 is in their correlation range. Given that the LD and LMC-WD models are

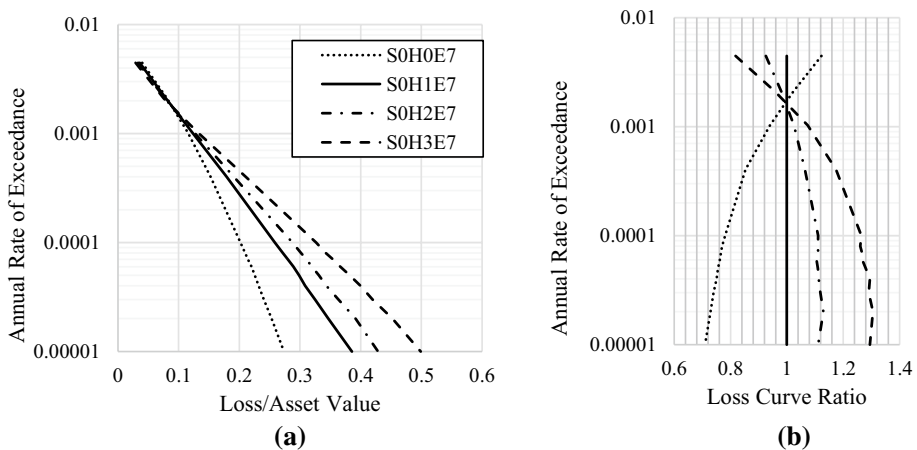


Fig. 6 **a** Normalized aggregated loss curve of exposure scenario E7 considering soil type S0 derived from different seismic hazard models, **b** The ratio of loss curves obtained from different hazard models to the loss curve obtained from the LD method

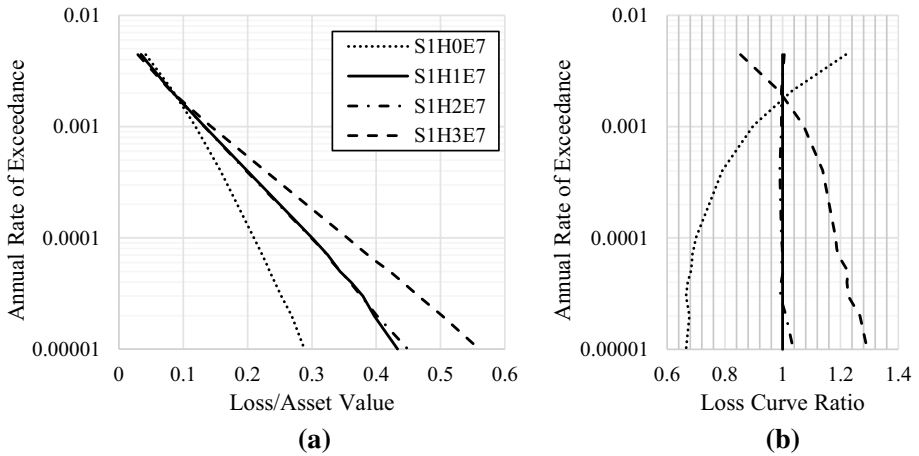


Fig. 7 **a** Normalized aggregated loss curve of exposure scenario E7 considering soil type S1 derived from different seismic hazard models, **b** The ratio of loss curves obtained from different hazard models to the loss curve obtained from the LD method

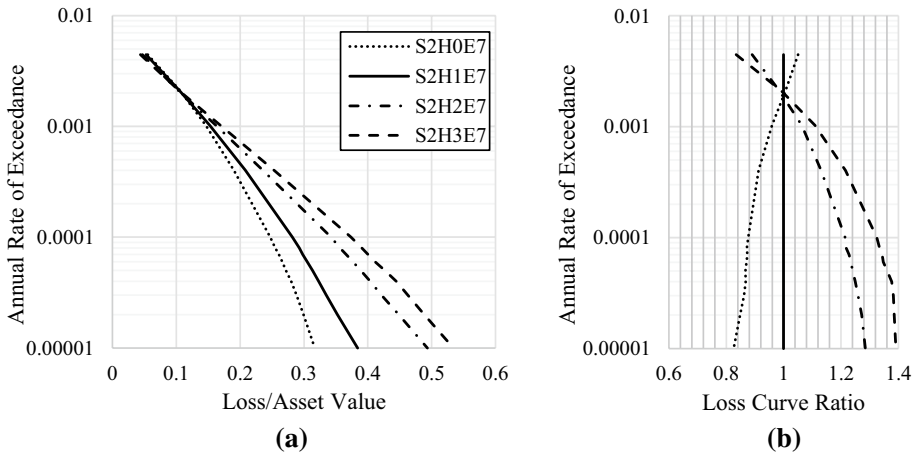


Fig. 8 **a** Normalized aggregated loss curve of exposure scenario E7 considering soil type S2 derived from different seismic hazard models, **b** The ratio of loss curves obtained from different hazard models to the loss curve obtained from the LD method

functions of the spatial correlation characteristics of soil type (while the Uncorrelated and LMC-LB models are not influenced by the soil type conditions), the ratio of loss values obtained by different hazard models is expected to differ as soil characteristics changes. In this regard, by considering the soil type scenarios S1 and S2, the loss curves of Figs. 7, 8 are obtained.

Figures 6, 7 and 8 show that the results of the Uncorrelated method can be considered as the lower bound loss values for infrequent events. Moreover, it can be concluded that the more spatially correlated the soil type, the more difference there will be between the results of the LD and Uncorrelated models. In such cases, however, the loss values obtained using the LD model would be closer to those obtained using the LMC-LB model. On the other hand, the more uncorrelated the soil type, the closer the loss values of the LD model to the loss values of the Uncorrelated model. Although by reducing the spatial correlation range of the soil type, a considerable reduction is observed in the results of the LMC-WD model, no significant change can be detected in the difference between the results of the Uncorrelated model and the result of the LMC-LB model. It is worth noting that the LMC-WD model consistently offers higher loss values than the LD model for the loss values with high return periods.

4.3 Investigating the effect of the presence of trend in the spatial distribution of building typologies on the results of seismic risk assessment

One of the potential situations in an urban area is the existence of trends in the type of buildings. The effect of trends in building typologies on the outcome of the seismic risk assessment of a portfolio of buildings in an urban area is discussed in the current section. The findings of the current section could be utilized in disaster risk reduction actions through the identification of intervention actions in an existing urban area and risk-sensitive land use planning. For this purpose, the exposure models E3 and E4 are used in combination with seismic hazard scenarios related to soil type S0. With 50 percent of STL01 and 50 percent of CON01 building typologies, both E3 and E4 models have equal asset values. The main difference between these models is that in scenario E3, the trend in the density of building typologies is in the N-S direction, while in scenario E4, it is in the E-W direction.

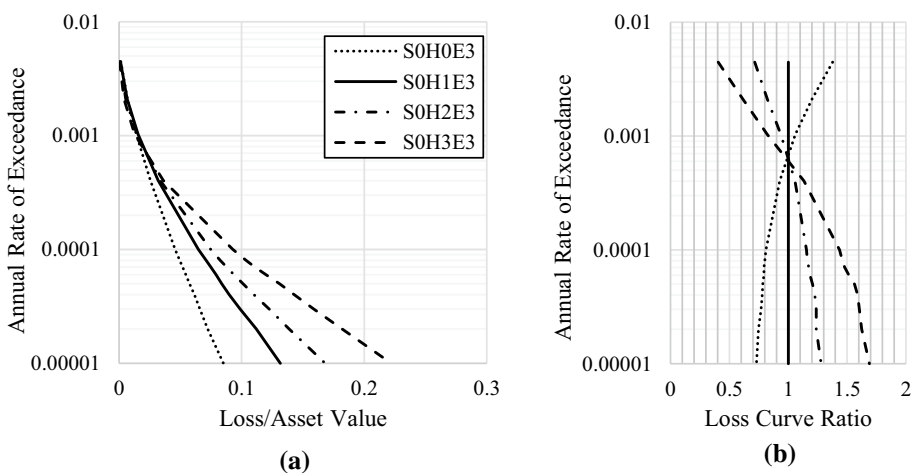


Fig. 9 **a** Normalized aggregated loss curve of exposure scenario E3 considering soil type S0 derived from different seismic hazard models, **b** The ratio of loss curves obtained from different hazard models to the loss curve obtained from the LD method

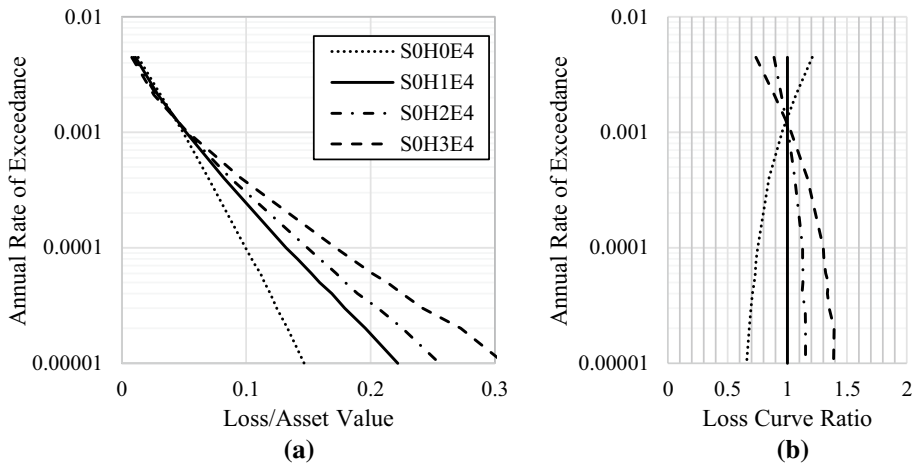


Fig. 10 **a** Normalized aggregated loss curve of exposure scenario E4 considering soil type S0 derived from different seismic hazard models, **b** The ratio of loss curves obtained from different hazard models to the loss curve obtained from the LD method

Figures 9, 10 depict the normalized loss curves of exposure models E3 and E4, respectively. At first, it should be noted that the total aggregated loss ratio of the E3 and E4 exposure models is less than the total aggregated loss ratio of the E7 exposure model, which is investigated in the previous section. The reduction in the loss values (in E3 and E4 compared to the E7) is due to the fact that the CON01 building typology, which its vulnerability is less than the STL01 building typology, accounts for half of the building stock in the E3 and E4 models, while the STL01 building typology accounts for all of the buildings in the E7 model.

Also, it is worth mentioning that the anisotropy direction of the regional site condition of Scenario S0 is aligned with the exposure model trend direction in the E3 exposure scenario while it is perpendicular to the exposure model trend direction in the E4 scenario.

If we consider the loss values of the LD method as the benchmark, it could be inferred from Figs. 9b, 10b that when the anisotropy direction of the regional site condition is aligned with the exposure model trend direction, the deviation of results obtained from other spatial correlation models (i.e., LMC-LB, LMC-WD models), that do not account for the anisotropy of spatial correlations of earthquake IMs, from the benchmark model (i.e., LD model) will be more than the case which the anisotropy direction of soil type and trend direction of exposure model are perpendicular to each other.

For instance, in the specific cases of exposure scenarios E3 and E4 in the current study, the loss ratio of LMC-WD (i.e., the ratio of estimated loss value obtained from the LMC-WD model to that estimated from the LD model) for 10^{-4} ARoE is about 1.44 in the E3 scenario, while it drops to 1.30 in E4 scenario. Also, the loss ratio of the LMC-LB model is about 1.16 for 10^{-4} ARoE in E3 exposure scenario, while it is approximately 1.12 in E4 exposure scenario.

The turning point of loss curve ratio charts is another parameter that significantly changed by altering the exposure scenario from E3 to E4. The turning point is defined as the ARoE at which a change occurs in the direction of the deviations of the loss values

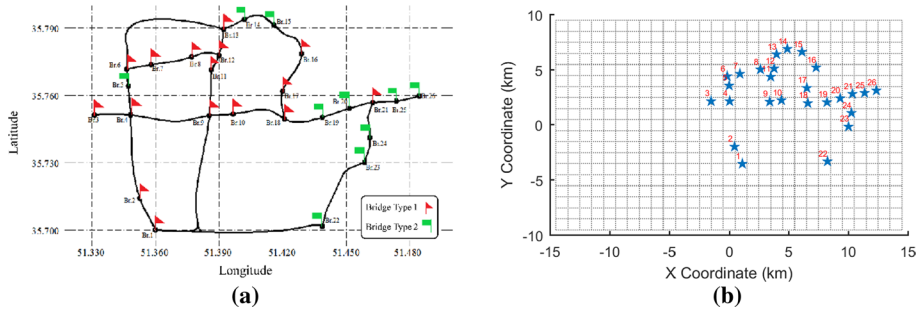


Fig. 11 **a** Spatial extend of the considered transportation network, **b** Location of the bridges in the assumed study area

Table 7 Characteristics of employed bridge typologies

Bridge Type	Fundamental Period (s)	LN [†] of the median value of SAs of different damage states [†]			
		Slight	Moderate	Extensive	Complete
BT1	0.5	- 0.29	0.18	0.5	0.93
BT2	1.0	- 0.69	- 0.22	0.1	0.53

[†]Natural Logarithm

[†]Values are derived from HAZAUS Technical Manual (FEMA 2015)

of isotropic models from the results of the benchmark model (LD model). For instance, the turning point of the exposure model E3 located in the S0 soil type scenario is about 4×10^{-4} in terms of ARoE (Fig. 9b), while the turning point of the exposure model E4 is about 1.2×10^{-4} (Fig. 10b). As can be seen from Figs. 9b and 10b, the turning point of loss curve ratio charts for the case in which the anisotropy direction is aligned with the exposure model trend direction is significantly lower than the turning point of loss curve ratio charts for the case in which the anisotropy direction is perpendicular to the exposure model trend direction.

The results of the current section emphasize the importance of identifying and taking into account the anisotropy direction of earthquake IMs when assessing the seismic risk of a trended exposure model or when renovating or extending an existing portfolio of buildings is of interest. This is especially important when the anisotropy direction of the regional site condition coincides with the trend direction of the exposure model. As a result, a spatial correlation model capable of incorporating the anisotropy of spatial correlations of earthquake IM should be employed.

5 Seismic risk and resilience assessment of the transportation network

5.1 Description of exposure and vulnerability models

The main objective of this section is to investigate the effect of utilizing different spatial correlation models of earthquake IMs on the result of seismic risk and resilience assessment of an infrastructure network. For this reason, the transportation network of Fig. 11a comprised of 26 bridges and their linking highways is considered. The depicted network is a part of the urban transportation network of the Tehran metropolitan area. Figure 11b shows the location of the considered network in the study area that is defined in Fig. 2. Moreover, the four spatial correlation models introduced in Sect.3.1 in conjugate with three regional site condition scenarios of S0, S1, and S2 defined in Sect. 3.2 are employed.

The bridges are classified into two types, and the vulnerability characteristics of each are displayed in Table 7. It should be noted that, while the type of bridges assumed in this example may differ from what actually exists in the mentioned transportation network, the main findings of the current research work are not dependent on the assumed typologies. The Slight, Moderate, Extensive and Complete damage states, which are mentioned in Table 7, indicate the mean damage ratio of 2%, 10%, 50% and 100%, respectively. Figure 11a presents the bridge types assigned to different bridge IDs in the assumed transportation network.

5.2 Investigating the seismic risk assessment results considering different spatial correlation models of earthquake IMs

The loss assessment of the introduced transportation network is conducted based on direct physical damage of bridge elements. In this regard, for the physical damages less than 50%, the direct economic loss value is assumed to be equal to the product of the physical damage ratio and total asset value, and for the physical damages more than 50%, the direct economic loss is assumed to be equal to 100% of asset value. The physical damage to links between bridges is ignored in this study.

Figure 12 presents the direct loss curves obtained based on the four different spatial correlation models considering the S0 soil type scenario. In this figure, the loss ratio is normalized to the total asset value. According to this figure, the LMC-WD model offers more

Fig. 12 Loss curves of transportation network considering soil type S0

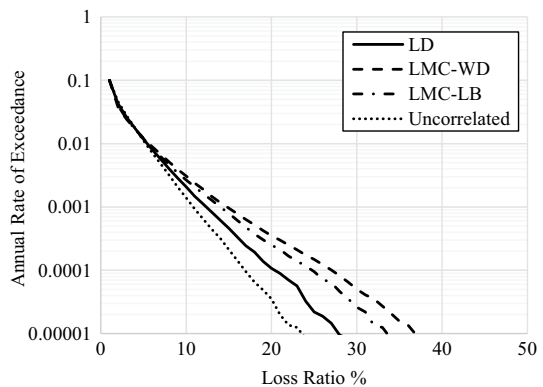


Fig. 13 Loss curves of transportation network considering soil type S1

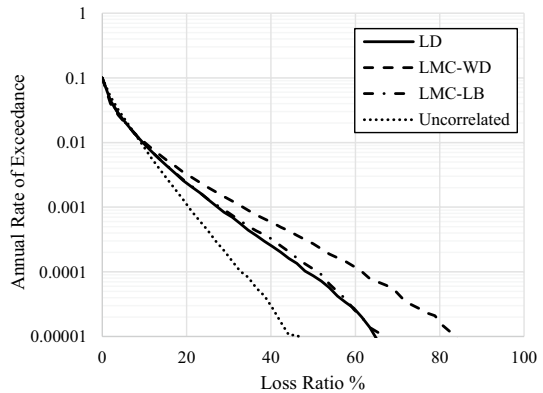
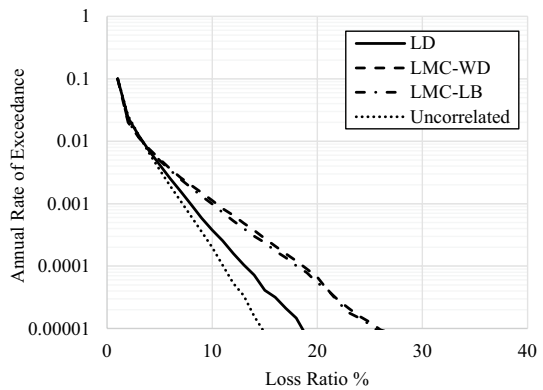


Fig. 14 Loss curves of transportation network considering soil type S2



loss ratios than those calculated by other models for rare events. Also, the loss ratio with high return periods calculated by the Uncorrelated model is less than the loss ratio calculated by other models. On the other hand, the LD model offers loss ratios between those proposed by the LMC-LB and Uncorrelated models.

The assumed transportation network is also evaluated under considerations of soil type scenarios S1 and S2 to examine the effects of various regional site conditions on the results of seismic loss assessment of infrastructure systems considering anisotropy of spatial correlation of earthquake IMs.

Figures 13 and 14 depict the loss curve of the transportation network, taking into account the S1 and S2 regional site condition scenarios, respectively. It should be noted in this section that by changing the soil type scenarios, considerable changes in the absolute V_{s30} value of the bridge locations may occur, resulting in a substantial change in the amount of earthquake IMs and, consequently, a considerable change in the amount of the loss values. For this reason, we do not compare the absolute loss ratios obtained from different soil type scenarios, but in this section, we are interested in relative loss ratios from different spatial correlation models in a single soil type model.

By comparing the results presented in Figs. 12, 13 and 14, it can be inferred that the infrequent loss values obtained from the LD model are always less than those obtained from the LMC-WD model. This is due to the fact that the LMC-WD model does not incorporate the anisotropy of spatial correlations and considers the identical correlation ranges

in different directions, while the correlation ranges considered by the LD model are different for various directions. As a result, the correlation range in specific directions is smaller than that considered by the isotropic model, while it is greater in other directions. This difference causes an overall reduction in the calculated loss values for events with a low frequency of occurrence.

Findings in Figs. 12, 13 and 14 also indicate that the LD method always offers more loss values than the Uncorrelated method (for infrequent events) and that the smaller the correlation range of soil type, the closer result of the LD method to the Uncorrelated method. On the other hand, the wider the correlation range of soil type, the closer the LD method result to the LMC-LB method results.

5.3 Investigating the seismic resilience assessment results considering different spatial correlation models of earthquake IMs

The current section investigates the effects of different spatial correlations models of seismic hazard IMs on the seismic resilience assessment of the infrastructure systems. For this purpose, the seismic resilience of the transportation network, presented in the previous section, is calculated using the approach introduced by Stergiou and Kiremidjian (2010). According to this approach, the transportation network’s seismic resilience is quantified by measuring its after-event performance relative to its original performance (performance before the occurrence of the destructive event). The performance of the network is quantified based on the performance of its link elements. To measure the original performance of the network, the average daily traffic (*ADT*) of the link elements is assumed to be 65’000 vehicles per day (veh/d), and the average traffic flow speed (*TF*) is assumed to be 40 km/h. Considering the mentioned values for *ADT* and *TF*, the normal daily traffic time (*NDTT*) of the entire network can be calculated as:

$$NDTT = \sum_{\text{all links}} ADT_i \times TF_i \times L_i, \tag{16}$$

where L_i is the length of link i and ADT_i and TF_i are average daily traffic and average traffic flow speed of link i , respectively. As demonstrated in Eq. (17), the damaged performance of each link is considered the worst case of damages of two bridges connected by the interested link.

$$Vul_L = \max \{ Vul_{Bs}, Vul_{Be} \}. \tag{17}$$

In Eq. (17), Vul_{Bs} and Vul_{Be} are the vulnerability ratios of bridges at two ends of the link and Vul_L indicates the vulnerability ratio of the interested link element. In this regard, the

Table 8 Repair/Reconstruction time of bridge components

Vulnerability ratio	Repair/Reconstruction time (day)
≤ 0.01	0
$0.01 \leq < 0.2$	4
$0.2 \leq < 0.5$	75
$0.5 <$	250

travel time in each link is increased according to its vulnerability ratio. The performance of the network in its disrupted state can be calculated in terms of the increased travel time as presented in Eq. (18).

$$DDTT = \sum_{\text{all links}} (1 + Vul_{L_i}) \times ADT_i \times TF_i \times L_i. \quad (18)$$

In Eq. (18), *DDTT* represents the disrupted daily traffic time, and other variables are defined previously. The current study assumes that the network's traffic demand is constant before and after the earthquake event, and investigating the variable traffic demand is out of the scope of the study. Based on calculated *NDTT* and *DDTT*, the dimensionless functionality loss of the entire network can be determined as:

$$FL = \frac{1}{NDTT}(DDTT - NDTT). \quad (19)$$

According to Bruneau et al. (2003), the resilience of a system is related to its functionality and recovery time. The current study uses the repair/reconstruction times of bridge components as a function of their vulnerability ratio, as presented in Table 8, to account for the transportation network's recovery (restoration) time in the calculations of system resilience.

In order to quantify the resilience of the transportation network, a time-history analysis approach based on the network functionality and restoration progress is conducted. The following steps present the employed approach:

1. A synthetic catalog with appropriate length is generated using the seismicity characteristics of the study area.
2. The GMF of scenario event *i* from the previously generated synthetic catalog is calculated. (To achieve the specific objectives of the current study, this step is carried out using four different spatial correlation models of 1-Uncorrelated, 2-LD, 3-LMC-WD, 4-LMC-LB and four resultant GMFs are obtained for each scenario event. Then, the following steps are conducted for each GMF separately.)
3. The vulnerability ratio of the bridge elements is calculated.
4. The functionality loss (*FL*) of the system and its functionality level at the first step of analysis ($F_0 = 1 - FL$) are calculated using Eq. (16) through Eq. (19).
5. The repair/reconstruction rate of each bridge is calculated based on its vulnerability ratio and repair/reconstruction time presented in Table 8.
6. Time-history analysis of network recovery is conducted. In this regard:
 - 6.1 The vulnerability level of each bridge on day *j* is obtained based on the bridge's vulnerability level on day *j*-1 and its repair/reconstruction rate.
 - 6.2 Based on the updated vulnerability ratio of bridges, the updated vulnerability ratio of links and consequently the updated functionality level of the network (F_j) is calculated.
 - 6.3 The procedure of step 5 is repeated (over the next *j* + 1 days) until all bridges have regained their original functionality level.
7. The previous steps are repeated until all scenario events from the generated synthetic catalog are included.

In the current study, three different soil type scenarios, described in the previous sections, are also employed, and consequently the entire time-history process is carried out

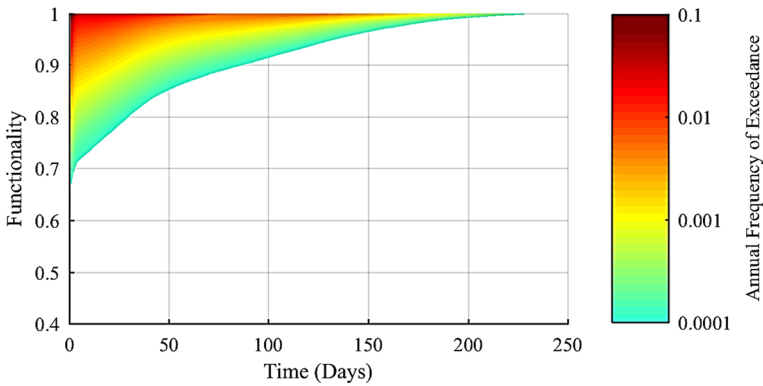


Fig. 15 2D visualization of a sample of resilience surface

Fig. 16 Resilience curve of the considered transportation system with 2475 years of return period under the assumption of S0 soil type scenario

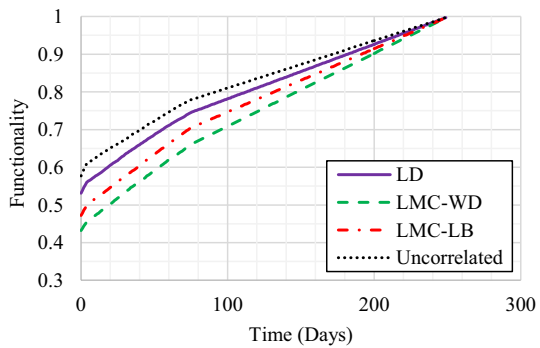
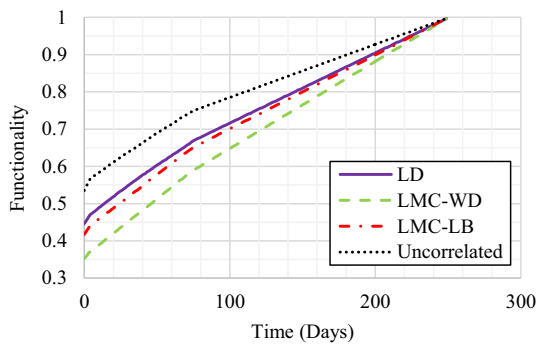


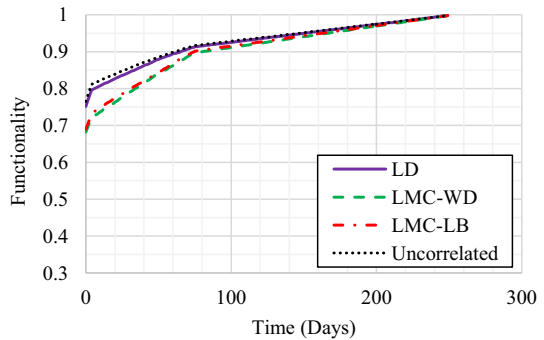
Fig. 17 Resilience curve of the considered transportation system with 2475 years of return period under the assumption of S1 soil type scenario



$4 \times 3 = 12$ times, taking into account different spatial correlation models and soil type scenarios.

Step 5 of the above-mentioned procedure provides the time-dependent functionality of the system (resilience diagram) for all scenario events of the synthetic catalog. Since the entire procedure is based on the Monte-Carlo simulation method, the expected functionality level of the system on the j th day after occurrence of the destructive event

Fig. 18 Resilience curve of the considered transportation system with 2475 years of return period under the assumption of S2 soil type scenario



can be determined for various ARoEs. In this regard, a 3D surface of functionality-time-ARoE is obtained as the "resilience surface". Figure 15 presents 2D visualization of a sample of resilience surface.

To investigate more precisely the effects of utilizing different spatial correlation models on the results of resiliency assessment of the system, resilience curves with a return period of 2475 years (ARoE of about 0.0004 or 2% probability of occurrence in 50 years) are extracted from resilience surfaces obtained from different spatial correlation models and are assessed in the following. Figure 16 presents the resilience curve of the considered transportation network with a return period of 2475 years for the case of the S0 soil type scenario. Also, Figs. 17 and 18 present the resilience curves of the transportation network considering S1 and S2 soil type scenarios, respectively.

According to the mentioned figures, by increasing the spatial correlation range of soil type (changing soil type scenario from S0 to S1), the resilience curve obtained from the LD method shifts away from results obtained from the Uncorrelated model toward the curve obtained from the LMC-LB model. Increasing the spatial correlation range of soil type also causes an increase in the difference between the results of LMC-WD and LMC-LB models. The main reason for this observation is that the LD and LMC-WD models include the spatial correlation range of soil type as a prerequisite factor in their estimation of GMF, while the Uncorrelated model and LMC-LB model estimate GMF without taking local soil type condition into account.

On the other hand, decreasing the spatial correlation range of soil type (changing the soil type scenario from S0 to S2) led the results of the LD method to be closer to the Uncorrelated model. Although the resilience curve obtained from the LMC-WD method has become closer to that obtained from the LMC-LB method and the Uncorrelated model, there is still a significant difference between the results obtained from the LMC methods (LMC-WD and LMC-LB) and the Uncorrelated model.

Suppose we consider the LD approach as the most accurate method among the utilized methods, capable of considering anisotropic spatial correlations and regional soil conditions. Consequently, it can be inferred from the obtained results that for the case of the low amount of spatial correlations of soil conditions, both of the LMC methods (LMC-WD and LMC-LB) overestimate the loss values and restoration time of the entire system that results in a low level of resilience curve. On the other hand, it can be concluded that the LMC-LB approach provides fairly reliable results in the case of a wide spatial correlation range of soil conditions, and the reliability of findings of the LMC-LB approach declines as the correlation range of soil type decreases.

6 Conclusion

The effect of considering anisotropy of spatial correlations of earthquake IMs on seismic risk and resilience assessment of spatially distributed assets is investigated in the current study. Three different multivariate spatial correlation models and an uncorrelated model are utilized. One of them is the latent dimension (LD) model proposed by Abbasnejad-fard et al. (2020) that is capable of considering the anisotropy of spatial correlations of IMs and regional site conditions. The other models which are proposed by Loth and Baker (2013) (LMC-LB) and Wang and Du (2013) (LMC-WD) are based on the linear model of coregionalization (LMC) and isotropic consideration. The LMC-WD model also can account for the regional site conditions. For this reason, three different soil type scenarios are generated, each with different spatial correlation properties of V_{S30} values. For the risk and resilience assessment objectives, the portfolio of residential buildings in a synthetic urban area and a transportation network are used.

Event-based probabilistic risk and resilience assessment conducted in the current study revealed that ignoring the anisotropy of spatial correlations of earthquake IMs would lead us to unrealistic results for loss and resilience values of spatially distributed assets and systems. It could be concluded that the isotropic models generally overestimate the rare loss and resilience values and underestimate the frequent results, particularly in the cases of heterogeneous soil conditions where the spatial correlation range of the V_{S30} is not substantial. The difference between isotropic and anisotropic models is due to the fact that the isotropic models consider the same correlation ranges in different directions, while the anisotropic models can incorporate the variable correlation ranges in different directions simultaneously. Consequently, for cases with a low anisotropy ratio, which is expected to occur in homogenous local site conditions, the results of the isotropic models will be closer to those of the anisotropic models.

From the practical usage point of view, it could be noted that if the objective of the risk and resilience assessment is to obtain only the consequences of infrequent events, the isotropic models present conservative results, although the results of isotropic models may be significantly erroneous, especially in the case of heterogeneous soil condition. However, if the objective of risk and resilience assessment is to obtain risk/resilience curves, calculate the results for a single scenario event, or calculate the average loss values across a specific time period, the isotropic models may provide unreliable results considering the fact that they underestimate the frequent losses.

It is worth mentioning that the LD and LMC-WD models mainly are functions of local site conditions, and utilizing these models needs the spatial correlation properties of local soil conditions to be identified. However, as mentioned in Abbasnejad-fard et al. (2020) and based on the evidence provided by other research works (e.g., Garakaninezhad and Bastami (2017) and Schiappapietra and Smerzini (2021)), earthquake source and path physical characteristics may have considerable effects on the anisotropy of the spatial correlations of IMs. In this regard, the mentioned parameters should be included in spatial correlation models based on the newly recorded data or earthquake simulation methods.

The current study also used different scenarios of exposure models of a building portfolio to evaluate how the configuration of the exposure models influences the degree of impact of incorporating anisotropy on risk assessment outcomes. The mentioned scenarios mainly focus on the presence of trend in building typologies which is prevalent in some of the urban areas where the city is extended or renovated in a particular direction.

It is demonstrated that when the anisotropy direction of IMs coincides with the trend direction of the exposure model, the deviation of isotropic spatial correlation models from the anisotropic model is more significant.

Acknowledgements The authors would like to acknowledge the International Institute of Earthquake Engineering and Seismology (IIEES) for the provided supports.

Authors' contribution Conceptualization: [MA, MB], Methodology: [MA], Formal analysis and investigation: [MA], Writing—original draft preparation: [MA]; Writing—review and editing: [MA, MB, AG], Funding acquisition: [MB], Resources: [MB], Supervision: [MB, AF], Project administration [MB], Software [MA], Visualization [MA].

Funding This work was supported by International Institute of Earthquake Engineering and Seismology (IIEES) under grant number 7552.

Data availability The data will be available as requested.

Code availability The utilized codes will be available as requested.

Declarations

Conflicts of interest The authors have no conflicts of interest to declare that are relevant to the content of this article.

References

- Abbasnejadfar M, Bastami M, Fallah A (2020) Investigation of anisotropic spatial correlations of intra-event residuals of multiple earthquake intensity measures using latent dimensions method. *Geophys J Int* 222:1449–1469. <https://doi.org/10.1093/gji/ggaa255>
- Apanasovich TV, Genton MG (2010) Cross-covariance functions for multivariate random fields based on latent dimensions. *Biometrika* 97:15–30. <https://doi.org/10.1093/biomet/asp078>
- Bastami M (2007) Seismic reliability of power supply system based on probabilistic approach. Kobe University, Japan
- Bastami M, Kowsari M (2014) Seismicity and seismic hazard assessment for greater Tehran region using Gumbel first asymptotic distribution. *Struct Eng Mech* 49:355–372
- Boore DM, Gibbs JF, Joyner WB et al (2003) Estimated ground motion from the 1994 Northridge, California, earthquake at the site of the interstate 10 and La Cienega Boulevard bridge collapse, West Los Angeles, California. *Bull Seismol Soc Am* 93:2737–2751. <https://doi.org/10.1785/0120020197>
- Bruneau M, Chang SE, Eguchi RT et al (2003) A framework to quantitatively assess and enhance the seismic resilience of communities. *Earthq Spectra* 19:733–752. <https://doi.org/10.1193/1.1623497>
- Campbell KW, Bozorgnia Y (2014) NGA-West2 ground motion model for the average horizontal components of PGA, PGV, and 5% damped linear acceleration response spectra. *Earthq Spectra* 30:1087–1114. <https://doi.org/10.1193/062913EQS175M>
- Cressie N (1993) Statistics for spatial data: Wiley series in probability and mathematical statistics. John Wiley & Sons
- Crowley H, Bommer JJ (2006) Modelling seismic hazard in earthquake loss models with spatially distributed exposure. *Bull Earthq Eng* 4:249–273. <https://doi.org/10.1007/s10518-006-9009-y>
- Du W, Wang G (2013) Intra-event spatial correlations for cumulative absolute velocity, arias intensity, and spectral accelerations based on regional site conditions. *Bull Seismol Soc Am* 103:1117–1129. <https://doi.org/10.1785/0120120185>
- Esposito S, Iervolino I (2011) PGA and PGV spatial correlation models based on European multievent datasets. *Bull Seismol Soc Am* 101:2532–2541
- Esposito S, Iervolino I (2012) Spatial correlation of spectral acceleration in European data. *Bull Seismol Soc Am* 102:2781–2788. <https://doi.org/10.1785/0120120068>
- FEMA (2015) Multi-hazard loss estimation methodology, earthquake model, Hazus–MH 2.1: technical manual. Federal Emergency Management Agency, Washington

- Garakaninezhad A, Bastami M (2017) A novel spatial correlation model based on anisotropy of earthquake ground-motion intensity. *Bull Seismol Soc Am* 107:2809–2820. <https://doi.org/10.1785/0120160367>
- Garakaninezhad A, Bastami M (2019) Intra-event spatial correlation model for the vertical component of response spectral accelerations. *J Seismol* 23:853–867
- Goda K, Atkinson GM (2009) Probabilistic characterization of spatially correlated response spectra for earthquakes in Japan. *Bull Seismol Soc Am* 99:3003–3020
- Goda K, Hong HP (2008a) Spatial correlation of peak ground motions and response spectra. *Bull Seismol Soc Am* 98:354–365. <https://doi.org/10.1785/0120070078>
- Goda K, Hong HP (2008b) Estimation of seismic loss for spatially distributed buildings. *Earthq Spectra* 24:889–910. <https://doi.org/10.1193/1.2983654>
- Jayaram N (2010) Probabilistic seismic lifeline risk assessment using efficient sampling and data reduction techniques. Stanford University
- Jayaram N, Baker JW (2008) Statistical tests of the joint distribution of spectral acceleration values. *Bull Seismol Soc Am* 98:2231–2243. <https://doi.org/10.1785/0120070208>
- Jayaram N, Baker JW (2009) Correlation model for spatially distributed ground-motion intensities. *Earthq Eng Struct Dyn* 38:1687–1708
- Lee R, Kiremidjian AS (2007) Uncertainty and correlation for loss assessment of spatially distributed systems. *Earthq Spectra* 23:753–770
- Loth C, Baker JW (2013) A spatial cross-correlation model of spectral accelerations at multiple periods. *Earthq Eng Struct Dyn* 42:397–417
- Park J, Bazzurro P, Baker JW (2007) Modeling spatial correlation of ground motion intensity measures for regional seismic hazard and portfolio loss estimation. *Appl Stat Probab Civ Eng* 1–8
- Sadeghi N, Ghafory-Ashtiany M, Pakdel-Lahiji N (2015) Developing seismic vulnerability curves for typical Iranian buildings. *Proc Inst Mech Eng Part O J Risk Reliab* 229:627–640
- Schiappapietra E, Douglas J (2020) Modelling the spatial correlation of earthquake ground motion: Insights from the literature, data from the 2016–2017 central Italy earthquake sequence and ground-motion simulations. *Earth Sci Rev* 203:103139. <https://doi.org/10.1016/j.earscirev.2020.103139>
- Schiappapietra E, Smerzini C (2021) Spatial correlation of broadband earthquake ground motion in Norcia (Central Italy) from physics-based simulations. *Bull Earthq Eng*. <https://doi.org/10.1007/s10518-021-01160-7>
- Silva V, Crowley H, Pagani M et al (2014) Development of the openquake engine, the global earthquake model's open-source software for seismic risk assessment. *Nat Hazards* 72:1409–1427
- Stergiou EC, Kiremidjian AS (2010) Risk assessment of transportation systems with network functionality losses. *Struct Infrastruct Eng* 6:111–125. <https://doi.org/10.1080/15732470802663839>
- Tavakoli B, Ghafory-Ashtiany M (1999) Seismic hazard assessment of Iran. *Ann Geophys*. <https://doi.org/10.4401/ag-3781>
- Wang G, Du W (2013) Spatial cross-correlation models for vector intensity measures (PGA, Ia, PGV, and SAs) considering regional site conditions. *Bull Seismol Soc Am* 103:3189–3204. <https://doi.org/10.1785/0120130061>
- Wang M, Takada T (2005) Macrospatial correlation model of seismic ground motions. *Earthq Spectra* 21:1137–1156
- Weatherill GA, Silva V, Crowley H, Bazzurro P (2015) Exploring the impact of spatial correlations and uncertainties for portfolio analysis in probabilistic seismic loss. *Bulletin of Earthquake Engineering* 13(4):957–981